LA-UR- 11-02733

Approved for public release; distribution is unlimited.

Title:	The Role of Monte Carlo Burnup Calculations in Quantifying Plutonium Mass in Spent Fuel Assemblies with Non-Destructive Assay
Author(s):	Jack D Galloway Stephen J Tobin Holly R Trellue Michael L Fensin
Intended for:	33rd ESARDA Annual Meeting Budapest, Hungary - 5/16/11 - 5/20/11

Los Alamos
NATIONAL LABORATORY
EST. 1943

Form 836 (7/06)

The Role of Monte Carlo Burnup Calculations in Quantifying Plutonium Mass in Spent Fuel Assemblies with Non-Destructive Assay

Jack D. Galloway, Stephen J. Tobin, Holly R. Trellue, and Michael L. Fensin

Los Alamos National Laboratory
Los Alamos, NM (87544) U.S.A.
E-mail: jackg@lanl.gov, tobin@lanl.gov, trellue@lanl.gov, mfensin@lanl.gov

Abstract:

The Next Generation Safeguards Initiate (NGSI) of the United States Department of Energy has funded a multi-laboratory/university collaboration to quantify plutonium content in spent fuel (SF) with non-destructive assay (NDA) techniques and quantify the capability of these NDA techniques to detect pin diversions from SF assemblies. The first Monte Carlo based spent fuel library (SFL) developed for the NGSI program contained information for 64 different types of SF assemblies (four initial enrichments, burnups, and cooling times). The maximum amount of fission products allowed to still model a 17x17 Westinghouse pressurized water reactor (PWR) fuel assembly with four regions per fuel pin was modelled. The number of fission products tracked was limited by the available memory. Studies have since indicated that additional fission product inclusion and asymmetric burning of the assembly is desired. Thus, an updated SFL has been developed using the Monte Carlo-based burnup code *Monteburns*, which links MCNPX to a depletion code and models a representative 1/8 core geometry containing one region per fuel pin in the assemblies of interest, including a majority of the fission products with available cross sections.

Often in safeguards, the limiting factor in the accuracy of NDA instruments is the quality of the working standard used in calibration. In the case of SF this is anticipated to also be true, particularly for several of the neutron techniques. The fissile isotopes of interest are co-mingled with neutron absorbers that alter the measured count rate. This paper will quantify how well working standards can be generated for PWR spent fuel assemblies and also describe the spatial plutonium distribution across an assembly. More specifically we will demonstrate how Monte Carlo gamma measurement simulations and a Monte Carlo burnup code can be used to characterize the emitted gamma spectrum and the asymmetries experienced in the second SFL.

Keywords: spent fuel, plutonium distribution, nuclear safeguards, non-destructive assay

1. Introduction

According to the Information Circular (INFCIRC) 153[1], the technical objective of International Nuclear Safeguards is "... the timely detection of diversion of significant quantities of nuclear material from peaceful nuclear activities ... and deterrence of such diversion by risk of early detection". In support of this objective a five year research effort was started in March, 2009, by the Next Generation Safeguard Initiative (NGSI) of the U.S. Department of Energy[2]. Initial efforts have been invested in Monte Carlo simulations of various detector designs. One item of great importance to the accurate assessment of the effectiveness of a particular detector design is the spent fuel composition in the fuel assembly being analyzed. The first phase of spent nuclear fuel modelling in support of the NGSI effort included significant effort by Fensin et al in the creation of Spent Fuel Library number 1 (SFL1)[3] using the MCNPX in-line burnup (BU) capabilities[4]. The simulation was performed using an infinitely reflected generic 17x17 PWR fuel bundle, utilizing 1/8 assembly symmetry. In an effort to more accurately capture the asymmetric spectral effects resulting from a fuel shuffling sequence, a second spent fuel library (SFL 2a)[5] has been developed which utilizes increased computational capabilities

coupled with new updates in MCNPX 2.7.d2 reducing memory requirements[6], allowing more realistic core shuffling sequences to be modeled. Using SFL 2a and two alternate shuffling sequences, pertaining to SFL 2b and 2c, which were simulated to provide additional data points for the assessment of spatial dependencies, spatial plutonium distribution and the dependence upon fuel shuffling schemes (core loading patterns) was investigated.

In addition to efforts invested in the characterization of plutonium in SFLs 2a, 2b and 2c, the asymmetric BU distribution also presented a more realistic starting point for performing passive gamma simulations in support of average BU estimation. Numerous studies have been performed investigating the accuracy of passive gamma measurements for BU determination including work by Hsue et al[7], Tsao and Pan[8], Fensin et al[9][12][13], and Phillips and Bosler[11]. In this study, the viability of coupled Monte Carlo based BU calculations with MCNPX detector simulations as applied to assemblies containing asymmetric spatial BU distributions is investigated.

2. Spent Fuel Library #2

The first spent fuel library created in support of the NGSI effort included a fully populated matrix consisting of four initial enrichments (IE) at 2, 3, 4 and 5%, four BU values of 15, 30, 45 and 60 GWd/MTU, and four cooling times (CT) of 1, 5, 20 and 80 years. In the creation of the second spent fuel library some data points were removed since they represented an unlikely domain space in typical reactor operation. The high BU, low IE data points, and all associated CTs of 2, 3% IE crossed with 45, 60 GWd/MTU were removed, as well as the 4% IE, 60 GWd/MTU data point. In place of these removed data points, the number of CT included with the remaining cases was increased and included 14 days, 1, 5, 20, 40 and 80 years.

Additionally, to characterize the plutonium density distribution across a single fuel pin in SFL 1, which was deemed important for x-ray fluorescence (XRF), each fuel pin in the infinitely reflected assembly was modeled with four independent BU rings. Given the need to quantify the consequent of shuffling an assembly throughout the core on all isotopes that impact NDA measurements, each fuel pin was modeled as one single BU region. This loss in spatial fidelity within each pin was necessary to accommodate the memory requirements for the fuel shuffling sequences, which require a greater number of burn materials.

2.1. SFL 2a, b, c Fuel Shuffling Sequences

Figure 1 Fuel Shuffling Sequence 1

Figure 1 shows the fuel shuffling sequence used to move fuel bundle #2 within the core, which corresponds to the fuel bundle used for isotopic information in this study. For fuel bundle #2, each pin was modeled as an independent fuel region, which due to computational limitations, still takes advantage of symmetry such that half of the 17x17 fuel assembly is modeled independently, pin by pin. Assembly 2 is located at the "Fresh UO_2 Fuel" location pertaining, and rotates through the once and twice irradiated positions. For the remaining assemblies in the core (1, 3-10) each assembly is depleted as one single burn region, where each pin is modeled separately for transport purposes.

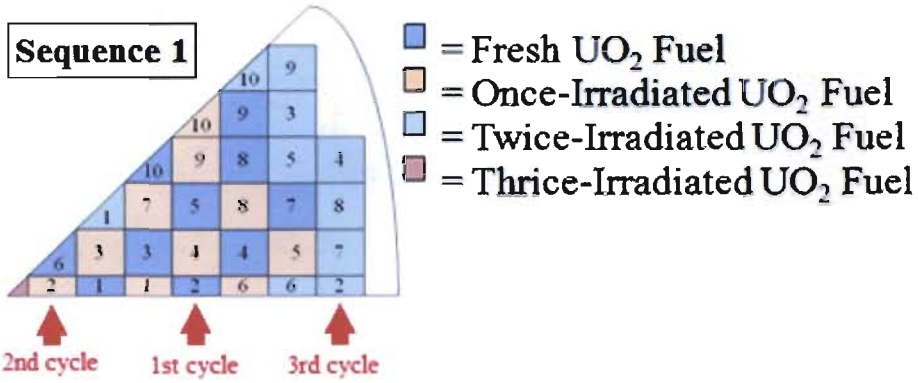

Figure 1 Fuel Shuffling Sequence 1 – Fuel Bundle #2

In addition to the initial shuffling sequence 1 shown in
Figure 1, two additional shuffling sequences, 2 and 3, were simulated to gather a better understanding of what differences may arise in plutonium concentration as well as fission product distributions as a result of variations in core loading patterns; they will be included in the distribution of SFL 2b and 2c. In
Figure 2, these two alternate fuel shuffling sequences are depicted and referred to as sequence 2 and sequence 3. These simulations are performed in the same fashion as the first sequence, with fuel type two having each pin depleted individually, and homogenous depletion for all other bundles, again where each pin is treated separately for transport considerations. These alternate fuel shuffling schemes were only performed for the 4% IE case, 15, 30, and 45 GWd/MTU as well as the same CTs listed above, since these were sensitivity studies intended to investigate spatial isotopic variations as a function of core loading patterns.

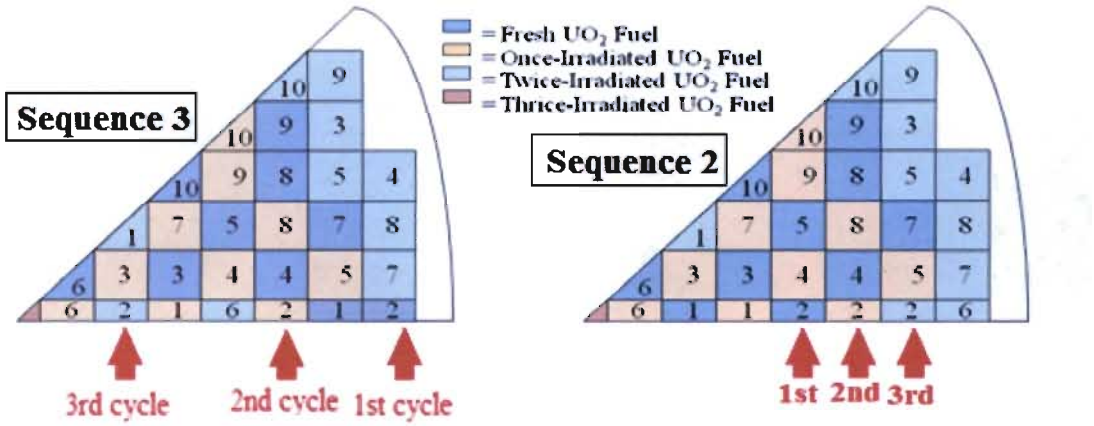

Figure 2 Shuffling Sequence 3 and 2 – Fuel Bundle #2

In traditional core loading patterns a choice of loading fresh fuel on the core periphery such as simulated in shuffling sequence 3 is a very atypical approach, however this simulation helps create a strong BU gradient across the bundle in cycle one. Thus, rotating this fuel into more reactive parts of the core serves to help quantify how strong an effect varying neutron flux gradients will have on an assembly, and in particular how strong the effect is on plutonium accumulation and the associated spatial distribution. The shuffling sequence in shuffling sequence 3, serves as a bounding condition up to 15 GWd/MTU, due to a fresh assembly adjacent to core periphery causing a high flux on the left boundary and high leakage causing a low flux off the assembly adjacent to the exterior of the core. Beyond 15 GWd/MTU for shuffling sequence 3 and for the full burn of shuffling sequence 2, a better

understanding of potential variations within the domain of viable core shuffling sequences is investigated.

3. Plutonium Distribution

The plutonium mass is the quantity upon which the accountancy system in the safeguards field is based. Using the three shuffling sequences described in the preceding section the radial plutonium distribution at the end of the first cycle, as well as at the end of cycle 3, is plotted in Figure 3, Figure 4, and Figure 5, pertaining respectively to fuel shuffling sequence one, shuffling sequence three and shuffling sequence 2.

In order to display the spatial plutonium distribution across the assembly, the zero plutonium concentrations in assembly locations that hold water rods (25 locations in total) were replaced by an average of the four surrounding fuel pins so that major discontinuities did not skew the visual depiction of the elemental spatial distribution.

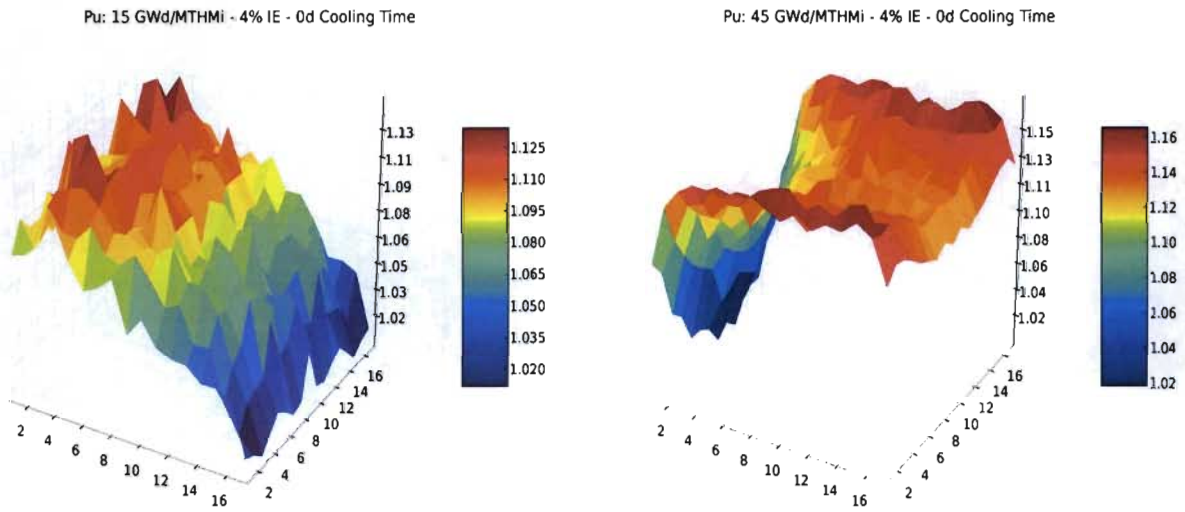

Figure 3 Shuffling Sequence 1 Pu Distribution – 15, 45 GWd/MTU

The scale on the z-axis, corresponding to plutonium mass, represents the maximum to minimum swing in plutonium mass across each assembly at each BU. This representation allows for a clear display of the magnitude of the plutonium gradient across the assembly due to the different shuffling schemes. In comparing Figure 3 and Figure 5, it is noted that in both shuffling sequences the fresh fuel started in nearly the same environment which resulted in very similar distributions at 15 GWd/MTU. In contrast, at 45 GWd/MTU the elemental gradients are somewhat mirror images. What is most interesting is that in both cases, while the spatial distribution deviated drastically being quite similar at 15 GWd/MTU and becoming close to mirror images at 45 GWd/MTU, the maximum to minimum swing in both cases was quite similar. In addition the comparison of total assembly plutonium shows a weak dependence upon the shuffling sequence, seen in

Elemental Pu Mass (g)	**Shuffle 1**	**Shuffle 3**	**Shuffle 2**
15 GWd/MTU	2708.07	2499.41	2662.54
% difference		-7.70%	-1.68%
45 GWd/MTU	5024.82	4983.85	5081.89
% difference		-0.82%	1.14%

Table 1 with the relative difference between the two total plutonium values being ~1% difference at both 15 and 45 GWd/MTU.

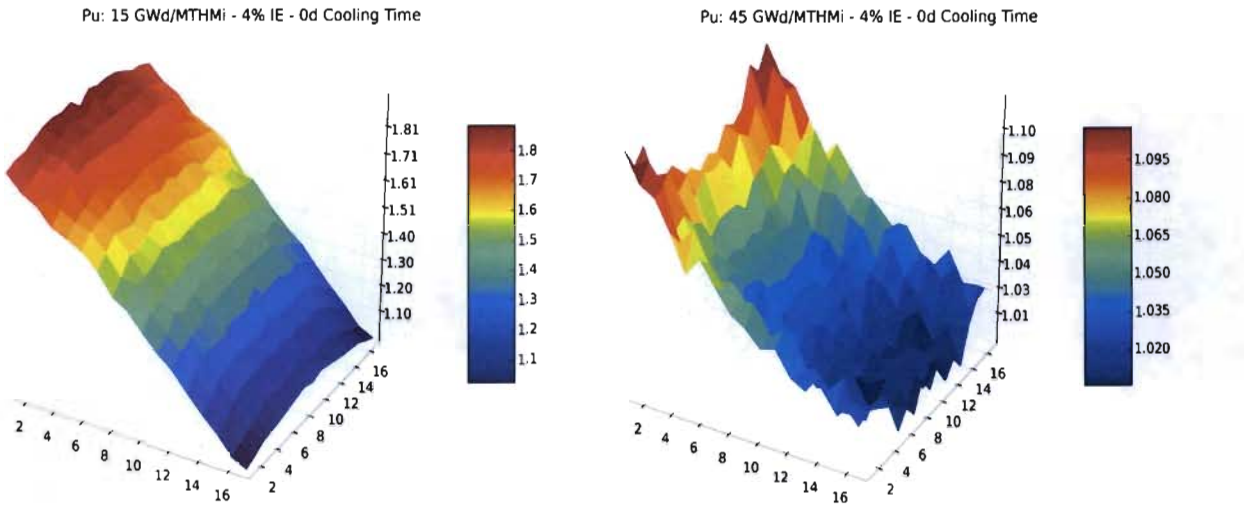

Figure 4 Shuffling Sequence 3 Pu Distribution – 15, 45 GWd/MTU

Figure 4 pertains to shuffling sequence 3 which started as fresh fuel on the exterior of the core and burned the fuel to 15 GWd/MTU before shuffling to a more internal location. While certainly a poor choice from a fuel cycle optimization stand point, this case allows for a better understanding of the effects of strong neutron flux gradients upon the accumulation of plutonium. Clearly the fuel shuffling sequence can have a significant impact upon the spatial distribution; in this extreme case at 15 GWd/MTU the plutonium swing reached ~1.8 whereas it had been ~1.13 for the two more traditional cases. This strong gradient also caused a 7.7% difference in total elemental plutonium mass compared to the total mas accumulated during shuffling sequence 1 for the same average burnup. In comparing the 45 GWd/MTU data for shuffling sequence 3 on Figure 4 and in Table 1, it should be recalled that this bundle was rotated into more central regions of the core for cycles two and three. By the time 45 GWd/MTU is reached, the maximum to minimum that had been ~1.8 had shrunk to 1.1, much more in-line with the two other shuffling sequence data at this same average BU. In addition while the relative difference between shuffling sequence 1 and shuffling sequence 3 was 7.7% at 15 GWd/MTU this value has also decreased fairly drastically to ~1.7% at 45 GWd/MTU.

Elemental Pu Mass (g)	**Shuffle 1**	**Shuffle 3**	**Shuffle 2**
15 GWd/MTU	2708.07	2499.41	2662.54
% difference		-7.70%	-1.68%
45 GWd/MTU	5024.82	4983.85	5081.89
% difference		-0.82%	1.14%

Table 1 Total Plutonium Mass (g)

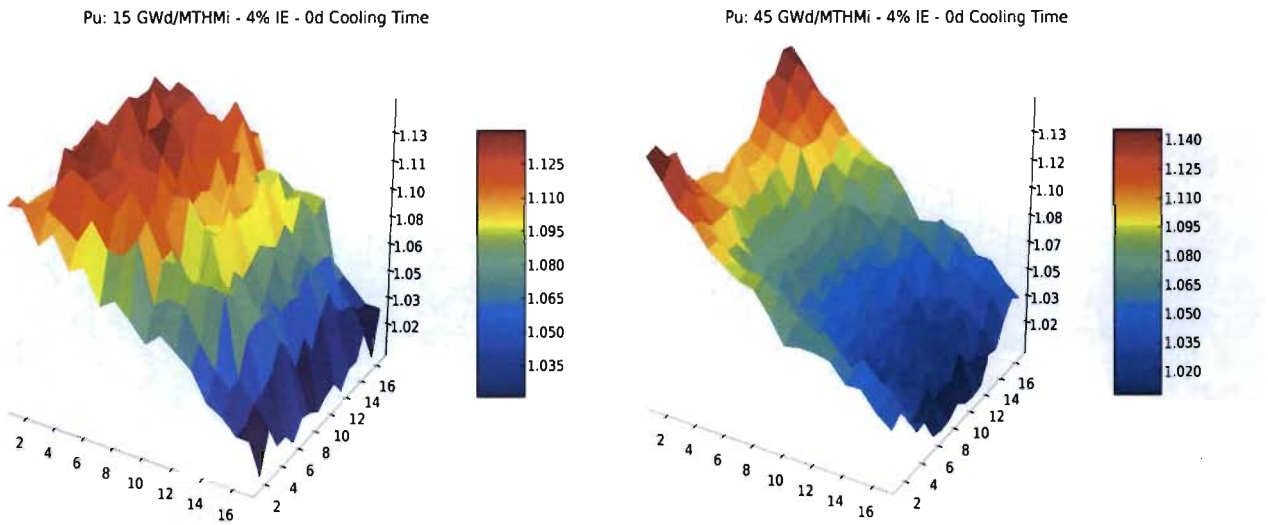

Figure 5 Shuffling Sequence 2 Pu Distribution – 15, 45 GWd/MTU

One trend consistent to all three shuffling sequences is that the highest plutonium content generally migrates to the perimeter of the assembly with increasing BU. Following the trend of the spatial distribution across the assembly, for any given row the largest elemental plutonium mass occurs at the assembly perimeter. The increased elemental plutonium mass is due primarily to the ^{239}Pu contribution, which is the single largest isotope contributing to elemental plutonium mass. The left most image in

Figure 6, is for shuffling sequence 1 while the right figure pertains to shuffling sequence 3, both cases are for 45 GWd/MTU and representing the spatial ^{239}Pu distribution. The ^{239}Pu is clearly concentrated higher on the edges than the internal regions of the fuel assembly, trending with the spatial distribution across the assembly.

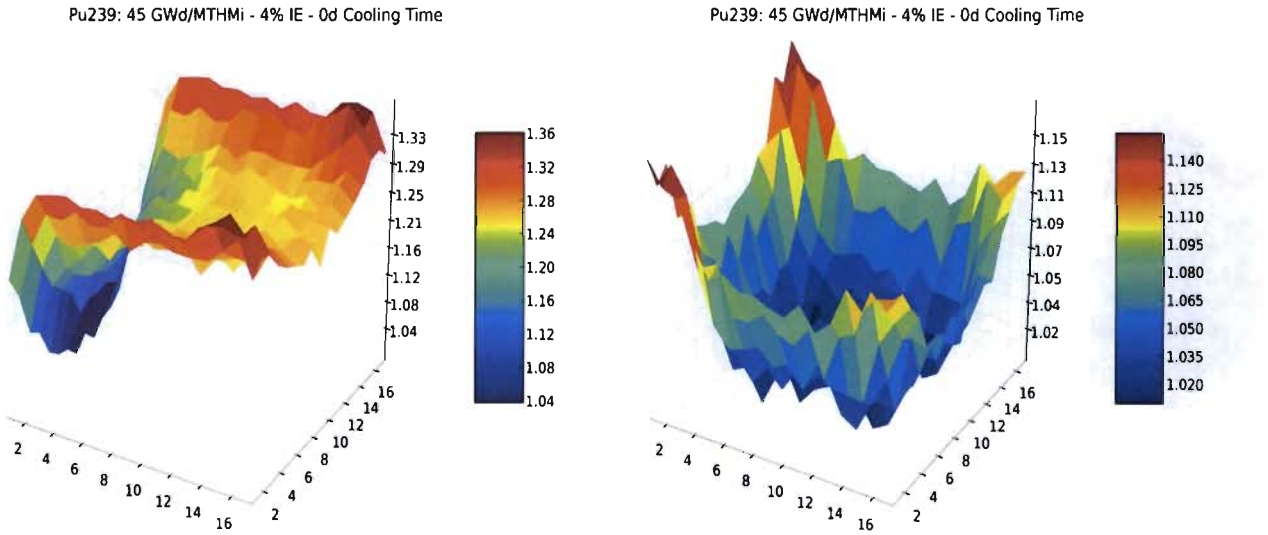

Figure 6 ^{239}Pu Concentration – Shuffling Sequence 1 (left), and Shuffling Sequence 3 (right) Both Images at 45 GWd/MTU

This ^{239}Pu spatial distribution drives the majority of the elemental plutonium spatial distribution, thus since the ^{239}Pu is preferentially weighted towards the edge of the assembly, the same trend holds true for elemental plutonium distribution.

45 GWd/MTU	**Sequence 1**	**Sequence 2**	**Sequence 3**
Pu (g)	5024.82	5081.89	4983.85
Pu239 (g)	2575.09	2682.90	2663.92
Pu239 % Contribution	***51.25%***	***52.79%***	***53.45%***
% Pu Change from Sequence 1		1.14%	-1.93%
% Pu239 Change from Sequence 1		4.19%	-0.71%

Table 2 shows the percentage contribution of elemental plutonium that ^{239}Pu is responsible for. For all three fuel shuffling schemes at end of life, 45 GWd/MTU, ^{239}Pu accounts for slightly greater than 50% of the elemental plutonium present in this assembly. Since this ^{239}Pu contribution is quite significant, and as seen in Figure 6, this ^{239}Pu is concentrated heavily around the assembly periphery, this combination causes the trend for elemental plutonium to also be weighted towards assembly periphery. It is however noted that the peak to minimum ratio in both cases, while weighted towards the assembly periphery, still has a noticeable dependence upon fuel rotation schemes. This is seen in the maximum to minimum ratio for the two cases shown in Figure 6, with the first swing being a factor of 1.36, while the second swing a much more moderate 1.15 for 45 GWd/MTU.

45 GWd/MTU	**Sequence 1**	**Sequence 2**	**Sequence 3**
Pu (g)	5024.82	5081.89	4983.85
Pu239 (g)	2575.09	2682.90	2663.92
Pu239 % Contribution	***51.25%***	***52.79%***	***53.45%***
% Pu Change from Sequence 1		1.14%	-1.93%
% Pu239 Change from Sequence 1		4.19%	-0.71%

Table 2 ^{239}Pu - Elemental Pu and ^{239}Pu Comparison

Lastly, seen in Table 2 is the variation in total assembly plutonium mass and ^{239}Pu mass due to the different core shuffling sequences, at 45 GWd/MTU. While ^{239}Pu has a greater difference, being as much as 4.2% for sequence 2, the elemental plutonium difference was less, where the 4.2% difference in ^{239}Pu only amounted to 1.14% difference in elemental plutonium. In an opposite trend for sequence 3, the ^{239}Pu difference was less than the elemental plutonium, being -0.71% and -1.93% respectively. These results indicate that the spectral history in which the BU was accumulated has an impact in how the isotopic vectors that constitute elemental plutonium are accumulated, as well as an impact in the total mass of elemental plutonium for a given BU.

4. Passive Gamma Simulations

The use of passive gamma techniques as an NDA technique for spent nuclear fuel has been investigated and used for BU determination for several decades now[7-13]. Given this pedigree, the passive gamma approach may be useful to the NGSI effort as part of an integrated instrument intended to detect the diversion of fuel pins, while also quantifying isotopic composition and being primarily interested in elemental plutonium concentration. In support of this effort, the capability to accurately measure the BU, IE and CT of an assembly is desired. The intent is to couple this passive gamma information with simulative data from other NDA techniques to provide an accurate estimate of plutonium mass in the assembly of interest. Initial studies in support of the NGSI initiative were performed by Fensin[9][12][13] which quantified the BU and IE determination capability for the first spent fuel library which was created for an infinitely reflected 1/8 symmetric assembly. Incurring the same spatial and isotopic characteristics discussed in section two above, an amended passive gamma simulative approach needed to be applied to the assembly used in the second SFL.

Due to the asymmetric effects introduced in a fuel shuffling sequence, passive gamma simulations were required on three sides of an assembly. For an implemented system, scans might be performed either on all four sides, the four corners of the assembly, or even more locations depending on how accurate a result was needed. In SFLs 2a,b,c there was still a computational limitation on the number of burn materials allowed, thus one-half assembly reflection required simulations on only three sides of the assembly. Figure 7 shows the geometry of the simulation setup that is often used in the field. An alternative approach being considered involves a wide collimator that allows the entire side of the SF assemblies to be measured at one time, which was simulated in this study.

The passive gamma geometry setup is a difficult radiation transport problem since the photons must reach a tiny detector located a very large number of mean free paths away. Also the diameter of the collimator tube is 5.08 cm which, in the context of the size of the bundle is quite small. As Fensin[9][12][13] discussed previously, the simulative approach adopted was to tally the flux crossing the entire assembly boundary adjacent to the collimator tube. This flux was then "pushed", or translated, up the collimator tube to the HPGE detector and a pulse-height tally was used to simulate the spectra. The same approach has been adopted for the first round of passive gamma calculations using the spatial isotopic distribution obtained from SFLs 2a,b,c.

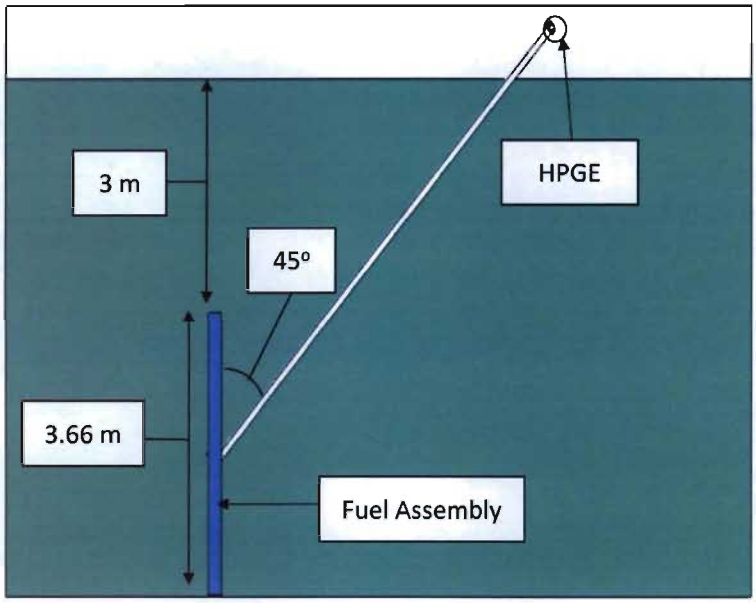

Figure 7 Passive gamma geometry

Given the simplifying assumptions made, it is expected that some inaccuracies have been introduced particularly in the magnitude of the continuum. However, given the extreme length of the collimator, the inaccuracies are not expected to be great. The resultant signal can be interpreted as proportional to the expected signal should a passive gamma scan be performed that spans the full length of each side of the assembly. In addition, a better understanding of the detection sensitivity to asymmetric effects introduced by the fuel rotation scheme, which was the initial primary objective, should result.

To tally the outgoing fluxes across assembly boundaries, a script was generated that serves as an automated process for first, computing the pin-wise gamma source file based upon the pin-by-pin isotopic compositions resulting from SFLs 2a,b,c and then creating the MCNPX input file with the combination of material compositions from SFLs 2a,b,c and the source calculation. This method is a modification and enhancement of the BAMF tool developed by Sandoval and Fensin[14]. Using this representative photon source, MCNPX tallies the energy dependent gamma lines crossing each boundary, which are then ultimately used in the creation of a final MCNPX deck which includes an f8 pulse-height tally to simulate a detectors response to the incoming gamma flux. This process can be run for every BU, IE and CT available in SFLs 2a,b,c, allowing for a wide suite of fuel rotation conditions which can serve well for assessing the potential for BU and IE determination.

Preliminary simulations have been performed to observe the variation in intensity of the gamma signal as a result of spatial BU distributions. The first case chosen to simulate was the 15 GWd/MTU case from shuffling sequence 3, data which was already illustrated in Figure 2 and Figure 4 above. This was chosen since it has the most extreme spatial gradient of any of the shuffling rotations simulated. Figure 8 shows the relative intensity spectrum for the five year CT case at 15 GWd/MTU. Although it is difficult to see due to the logarithmic scale, the detector associated with "side 2", corresponding to the highest burnt side of the assembly, also experienced the strongest gross signal.

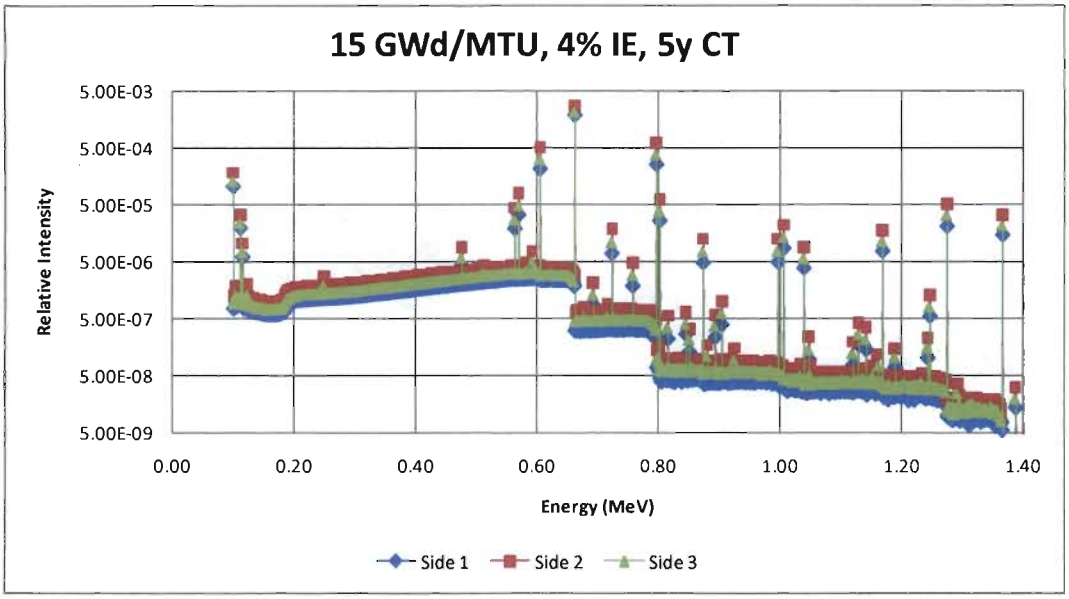

Figure 8 Relative intensity vs. energy (MeV) – 15 GWd/MTU – 5y CT

Relative difference from side 2 activity (5y cooling time)		
	Side 1	Side 3
Cs-134 (.6047 MeV)	-40.86%	-58.84%
Cs-137 (0.6617 MeV)	-23.86%	-32.49%
Cs-134 (0.7959 MeV)	-39.55%	-58.39%

Table 3 Relative difference – 15 GWd/MTU – 5y CT

In quantifiable terms,

Relative difference from side 2 activity (5y cooling time)		
	Side 1	Side 3
Cs-134 (.6047 MeV)	-40.86%	-58.84%
Cs-137 (0.6617 MeV)	-23.86%	-32.49%
Cs-134 (0.7959 MeV)	-39.55%	-58.39%

Table 3 shows the percentage differences for the three most prominent peaks, the 662 keV line from ^{137}Cs, and two ^{134}Cs lines at 605 keV and 796 keV. From Table 3 it is apparent that the ^{134}Cs peaks have a stronger dependence on the assembly spatial power distribution than the ^{137}Cs peak, having nearly double the percentage difference than the variation seen in the ^{137}Cs peak intensity. This result

is as expected since ^{134}Cs accumulation scales closely with the square of the flux, whereas the ^{137}Cs accumulation scales linearly with the flux.

Equation 1 and Equation 2 show the decay chains upon which ^{137}Cs and ^{134}Cs production depend, keeping in mind that both chains are initially dependent upon the flux through the fission product yields of each isotope in the decay chains. In the case of ^{134}Cs the second dependence on flux comes through the capture reaction of ^{133}Cs to ^{134}Cs, and this additional dependence causes the greater variation in signal intensity for ^{134}Cs seen in

Relative difference from side 2 activity (5y cooling time)		
	Side 1	Side 3
Cs-134 (.6047 MeV)	-40.86%	-58.84%
Cs-137 (0.6617 MeV)	-23.86%	-32.49%
Cs-134 (0.7959 MeV)	-39.55%	-58.39%

Table 3. The edge of the bundle that was located on the core periphery received much less of a flux intensity than the internal edge due to leakage, causing the greater signal intensity differences in ^{134}Cs when compared to ^{137}Cs which only depends on the flux through fission yields.

$$137_I \rightarrow 137_{Xe} \rightarrow 137_{Cs} \rightarrow 137_{Ba^m} \rightarrow 137_{Ba}$$

Equation 1 ^{137}Cs production chain

$$133_I \rightarrow 133_{Xe} \rightarrow 133_{Cs(n,\gamma)}134_{Cs} \rightarrow 134_{Ba}$$

Equation 2 ^{134}Cs production

Figure 9 shows the relative gamma intensity as a function of energy for the 45 GWd/MTU, 4% IE and five year CT case from the shuffling sequence 1. Quite different from the preceding spectrum, the minimum-to-maximum swing in plutonium concentration for this case, seen in Figure 3, was much lower than the preceding case, being on the order of 15% as opposed to 80%. This indicates a more even power distribution across the assembly, which is also observed in Figure 9. Here it becomes very hard to visually distinguish the three spectra from each other, where the side 1 spectrum is, for the most part, hidden behind the other two.

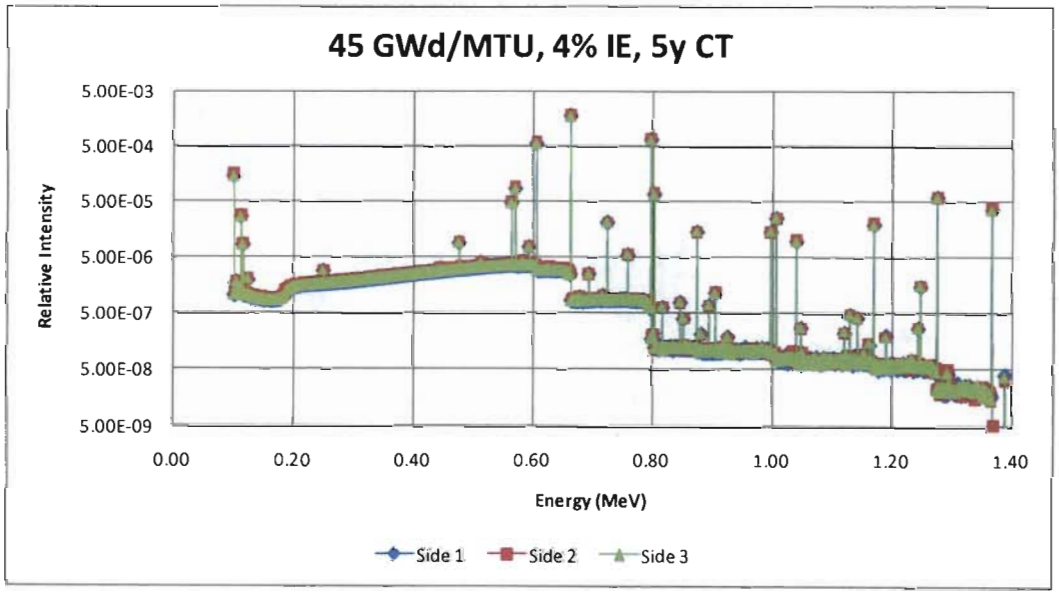

Figure 9 Relative intensity vs. energy (MeV) – 45 GWd/MTU – 1y CT

The percentage differences, relative to the maximum activity which again occurred across side 2, are much lower than in the previous case. Observed in Table 4, for all three isotope lines the largest difference occurred on side 1, varying from ~5-7%. There is clearly spatial sensitivity, largely influenced by the core loading patterns, which was also observed by trending the differences at each BU step for shuffling sequence 1. In this case differences of ~16% were observed for ^{134}Cs lines, and 8% for ^{137}Cs at 15 GWd/MTU. After the fuel was shuffled and continued burn to 30 GWd/MTU, the bundle moved to a further centrally located slot which served to create a more evenly distributed burn, and differences in ^{134}Cs lines have been reduced to ~4% with ~2.5% differences observed in ^{137}Cs. From there the bundle was shuffled to the core periphery where the differences grew, due to the exterior of the bundle having a large leakage term with virtually no incoming flux. The percent differences observed here were 5-7% in both ^{134}Cs and ^{137}Cs.

Relative difference from side 2 activity (5y cooling time)		
	Side 1	Side 3
Cs-134 (.6047 MeV)	-6.51%	-3.88%
Cs-137 (0.6617 MeV)	-5.21%	-4.51%
Cs-134 (0.7959 MeV)	-5.86%	-3.40%

Table 4 Relative difference – 45 GWd/MTU – 5y CT

With a half-life of 2 years, a significant portion of the ^{134}Cs has decayed by the time the 5y data was extracted, thus intensities are greater for gamma lines from ^{134}Cs at shorter CTs. Also, while there is a clear dependence upon the core shuffling sequence such that signal intensity differences amongst the sides of the bundle may be moderately larger at a higher BU compared to a lower BU, there also is a general trend of the relative differences amongst the sides trending from greater values to lesser values as BU increases, which arises from the reactivity characteristics of a bundle in the core. If one part of the bundle has been burned at a faster rate, in general as the bundle rotates throughout a typical shuffling sequence, the BU distribution across the bundle will tend to smooth out since there will be more fissile material in the under burned part of the bundle and power generation will eventually shift to the under-burned portion of the bundle. Again this is somewhat dependent upon shuffling sequence, but will hold true for typical fuel shuffling schemes. Thus, typically, high BU assemblies will not have the largest differences in signal intensity across the bundle from passive gamma measurements unless anomalous fuel shuffling practices are employed. This effect is observed in the case of the three BU points for shuffling sequence 1. The bundle rotated from one central location, to a more central location, til finishing its life on the core periphery. Despite the fact that strong asymmetries were experienced in the final shuffling sequence where high leakage occurred on one boundary, the relative difference at 45 GWd/MTU was significantly less than at 15 GWd/MTU, being ~16% at 15 GWd/MTU compared to ~6% at 45 GWd/MTU.

Comparing the ratio of ^{134}Cs/^{137}Cs a clear spatial dependence is evident for the strongly asymmetrically burned assembly. Using shuffling sequence 3 results at 15 GWd/MTU shuffling sequence 1 results at 45 GWd/MTU,

Sequence 3 - 15 GWd/MTU - 5y			
	cs134	cs137	**ratio**
Side 1	5.43E-04	1.84E-03	**0.2955**
Side 2	1.31E-03	2.72E-03	**0.4801**
Side 3	7.84E-04	2.07E-03	**0.3784**

Sequence 1 - 45 GWd/MTU - 5y			
	cs134	cs137	**ratio**
Side 1	1.37E-03	1.69E-03	**0.8100**
Side 2	1.46E-03	1.79E-03	**0.8178**
Side 3	1.41E-03	1.71E-03	**0.8258**

Table 5 shows the calculated Cesium ratios for these two cases. The data used to compute the ^{134}Cs contribution was a sum of all gamma lines emitted. The ratios from shuffling sequence 3 have a large variation, with side 1 being nearly 40% less intense than side 2, and side 3 being ~20% less intense than side 2. In contrast, shuffling sequence 1 only had a maximum difference of 2% between the most intense and least intense signals. Using this data combined with the isotopic information of each pin, it is possible that a relationship between the Cesium ratios and the plutonium content of the pins

contributing to the signal could exist, allowing the estimation of plutonium content in the fuel pins contributing to the passive gamma signal.

Sequence 3 - 15 GWd/MTU - 5y			
	cs134	cs137	ratio
Side 1	5.43E-04	1.84E-03	**0.2955**
Side 2	1.31E-03	2.72E-03	**0.4801**
Side 3	7.84E-04	2.07E-03	**0.3784**

Sequence 1 - 45 GWd/MTU - 5y			
	cs134	cs137	ratio
Side 1	1.37E-03	1.69E-03	**0.8100**
Side 2	1.46E-03	1.79E-03	**0.8178**
Side 3	1.41E-03	1.71E-03	**0.8258**

Table 5 Cesium Ratios

5. Future Work

Much work has gone into the generation of SFLs 2a,b,c, in an attempt to generate source signals that closely represent true conditions expected from a PWR 17x17 assembly. In leveraging this library for plutonium distribution studies it was observed that as BU increases, plutonium content not only increases but tends to have higher concentrations on bundle edges, and particularly bundle corners. Using known plutonium concentration from SFL 1 and SFLs 2a,b,c, particularly the edge concentration, to predict internal plutonium concentration, both in a spatial pin-by-pin distribution as well as a bundle total quantity of plutonium from the edge plutonium concentration would be useful in support of additional integrated instrument design in support of the NGSI initiative, particularly related to XRF instrument design and assessment. In addition, while passive gamma simulations of the total edge gamma flux benefit in understanding source magnitude differences as a result of shuffling schemes, more concentrated simulations attempting to simulate what the signal the HPGE detector would see would be beneficial, and allow the better estimations of how many locations, and which locations, would be needed to reliably extrapolate from passive gamma signal to an estimation of assembly average BU. Clearly multi-sided simulations would need to be performed for this task, but how many locations per side are needed, and where are the most important points to scan? These questions would need to be addressed to attempt to reliably use this technique to predict assembly average BU. In addition there is also a potential for using the passive gamma signal to calculate Cesium ratios which may be provide an accurate estimate for plutonium concentration in the fuel pins contributing to the passive gamma signal. A characterization of which pins contribute, and how much each pin contributes, to the total passive gamma signal for a given geometrical set up needs to be performed to better estimate the total plutonium content in those contributing pins.

6. Acknowledgements

The authors would like to acknowledge all those who have contributed to the NGSI effort, in particular to the Next Generation Safeguards Initiative, Office of Nuclear Safeguards & Security (NA-241), National Nuclear Security Administration in the U.S. Department of Energy for their support throughout this effort.

7 Legal matters

7.1. Privacy regulations and protection of personal data

"I agree that ESARDA may print my name and contact information as well as this paper in the ESARDA Bulletin and/or Symposium proceedings or any other ESARDA publication, and when necessary for any other purposes connected with ESARDA activities."

8. References

[1] IAEA Information Circular (INFCIRC)153 paragraph 28

[2] A. Scheinman, Next *Generation Safeguards Initiative Inaugural Conference, September 11-12, 2008* - http://nnsa.energy.gov/nuclear_nonproliferation /2147.htm
[3] M. L. Fensin, S. J. Tobin, N. P. Sandoval, S. J. Thompson, M. T. Swinhoe, "A Monte Carlo Linked Depletion Spent Fuel Library for Assessing Varied Nondestructive Assay Techniques for Nuclear Safeguards," Los Alamos National Laboratory Report: Full Paper: LA-UR 09-01188, American Nuclear Society's Advances in Nuclear Fuel Management IV, Hilton Head Island, South Carolina (April 12-15, 2009).
[4] M. L. Fensin, J. S. Hendricks, S. Anghaie, "The Enhancements and Testing for the MCNPX 2.6.0 Depletion Capability," Journal of Nuclear Technology, 170, pp. 68-79 (April 2010).
[5] Holly R. Trellue, et. al., "Description of Irradiated UO2 Fuel Compositions Generated for NGSI Spent Fuel Libraries", LA-UR 11-0030 (January 2011).
[6] M. L. Fensin, "MCNPX Memory Reduction Patch—FY 2009," Los Alamos National Laboratory Report: LA-UR-09-06308 (October 2009).
[7] S. T. Hsue, T. W. Crane, W. L. Talbert, J. C. Lee, "Nondestructive Assay Methods for Irradiated Nuclear Fuels," *LA-6923*, Los Alamos, NM (1978).
[8] C. S. Tsao and L. K. Pan, "Reevaluation of the Burnup of Spent Fuel Pins by the Activity Ratio of $^{134}Cs/^{137}Cs$," *Application of Radiation and Isotopes*, **44**, pg. 1041-1046 (1993).
[9] M. L. Fensin, S. J. Tobin, M. T. Swinhoe, H. O. Menlove, "Quantifying the Passive Gamma Signal from Spent Nuclear Fuel in Support of Determining the Plutonium Content in Spent Fuel with Nondestructive Assay," *Institute of Nuclear Materials Management 50th Annual Meeting*, Tucson, AZ (July 12-16, 2009).
[10] D. Reily, N. Ensslin H. Smith, and S. Kreiner, *Passive Nondestructive Assay of Nuclear Materials*, NUREG/CR-5550, Washington, DC (1991)
[11] J. R. Phillips and G. E. Bosler, "Calculated Response Contributions of Gamma Rays Emitted from Fuel Pins in an Irradiated PWR Fuel Assembly," *LA-9837-MS*, Los Alamos, NM (1994).
[12] M. L. Fensin, W. E. Koehler, S. J. Tobin, "MCNPX Simulation of a Passive Prompt Gamma System to be Used in a Spent Fuel Plutonium Assay Strategy," Los Alamos National Laboratory Report: LA-UR-10-00074, American Nuclear Society's Annual Meeting, San Diego, California (June 13–17, 2010).
[13] Michael L. Fensin, Stephen J. Tobin, Martyn T. Swinhoe, Howard O. Menlove, Will Koehler, Nathan P. Sandoval, Sang Lee, Vladimir Mozin, Josh Richard, Melissa Schear, Jianwei Hu, and Jeremy Conlin, "Determining the Pu Mass in LEU Spent Fuel Assemblies – Focus on Passive Gamma Detection," Los Alamos National Laboratory: LA-UR-11-00511 (January 2011).
[14] N. P. Sandoval and M. L. Fensin, "Burnup Automation MCNPX File Data Retrieval Tool (BAMF-DRT): Data Extraction and Input File Creation Tool Users Manual," *LA-UR-09-01259*, Los Alamos, NM (2008).